Front. Chem. Sci. Eng. 2020, 14(2): 216–232
https://doi.org/10.1007/s11705-019-1857-5

REVIEW ARTICLE

# Metal-organic framework UiO-66 membranes

**Xinlei Liu (✉)**

Catalysis Engineering, Department of Chemical Engineering, Delft University of Technology, 2629 HZ Delft, The Netherlands



**Abstract** Metal-organic frameworks (MOFs) have emerged as a class of promising membrane materials. UiO-66 is a prototypical and stable MOF material with a number of analogues. In this article, we review five approaches for fabricating UiO-66 polycrystalline membranes including *in situ* synthesis, secondary synthesis, biphase synthesis, gas-phase deposition and electrochemical deposition, as well as their applications in gas separation, pervaporation, nanofiltration and ion separation. On this basis, we propose possible methods for scalable synthesis of UiO-66 membranes and their potential separation applications in the future.

**Keywords** membrane, metal-organic framework, UiO-66, separation

## 1 Introduction

A vigorous search for novel membrane materials has been stimulated by the growing demand of energy-efficient separations [1–3]. Polymer membranes have been extensively investigated and applied in industrial gas separation [4], reverse osmosis [5], etc. due to their easy processing and mechanical strength. Inorganic membranes, for instance, zeolite membranes, have been successfully used for organic dehydration [6]. However, polymer membranes always suffer from low chemical and thermal stability, while zeolite membranes possess issues of brittleness, limiting their applications. Metal-organic frameworks (MOFs) [7], a class of hybrid materials constructed by coordinating metal-containing units with organic ligands, have received tremendous attention from membrane scientists in virtue of their versatile topologies and customizable chemistry. The teams of Caro [8] and Kapteijn [9] reported the earliest Metal-organic framework (MOF) films in 2007 and 2008, respectively, and later on in 2009, a few MOF membranes were explored for gas separation [10–15]. In the past 10 years, targeting to various separations, a booming development of MOF membranes has taken place. MOF-5, HKUST-1, IRMOF, ZIF, MIL and CAU membranes have been studied extensively [6,16–22]. However, they were always accompanied by concerns about the hydrothermal and chemical stability [23], which ultimately limited their further application in industries.

Recently, zirconium(IV)-carboxylate MOFs (Zr-MOFs) [24] have emerged as promising membrane materials due to their exceptionally high stability. According to Pearson's hard/soft acid/base principle [25], strong coordination bonds are expected by joining $Zr^{4+}$ (hard Lewis acid) and carboxylate based ligands (hard Lewis base) to determine the thermodynamic stability of Zr-MOFs. Besides, tetravalent Zr ions require more ligands to balance their charge and thus highly connected frameworks are formed with sufficient steric hindrance against attacks, which guarantees the structural stability from the kinetic aspect [26].

UiO-66 (UiO stands for University of Oslo) [27] is a prototypical and pioneered Zr-MOF, with the formula $Zr_6O_4(OH)_4(BDC)_6$ (BDC = 1,4-benzene-dicarboxylate) (Fig. 1(a)). It was firstly reported by Lillerud's group [27]. The inorganic brick of UiO-66 consists of a secondary building unit (SBU) $Zr_6O_4(OH)_4$ core, bridged by 12 carboxylates ($-CO_2$) originating from the dicarboxylic acids forming a face-centred cubic lattice (fcu topology). The diameters of the octahedral and tetrahedral cavities are ~1.1 and ~0.9 nm, respectively, and the triangular aperture size is ~0.6 nm as estimated from crystallographic data (Fig. 1(b)) [27,28]. Since its discovery in 2008, UiO-66 has been extensively investigated in the synthesis of its analogues [29]. Tetravalent metal ions (Fig. 1(c)) and BDC type ligands (Fig. 1(d)) were attempted to add to the family members of UiO-66. More than 40 of UiO-66 analogues have been confirmed [29]. Over the last few years, UiO-66 has almost dethroned MOF-5, HKUST-1, ZIF-8 and MIL-101 as a benchmark MOF material.

There are two main types of UiO-66 membranes: supported polycrystalline membranes and mixed matrix

Received March 19, 2019; accepted May 14, 2019

E-mail: x.liu-8@tudelft.nl

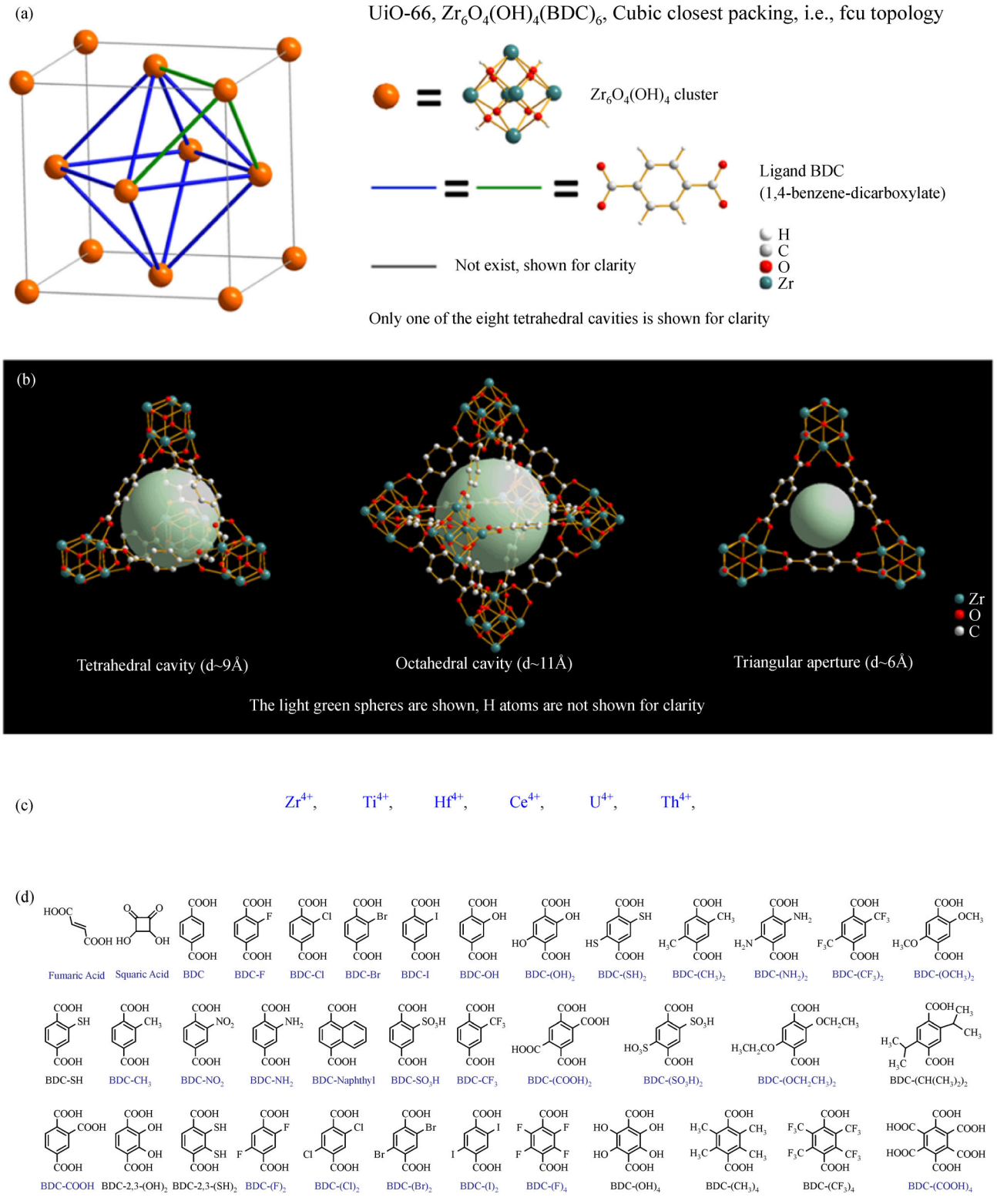


**Fig. 1** (a) The unit cell of UiO-66 constructed with $Zr_6$ cluster and BDC ligand. (b) The structure of UiO-66 cavities and aperture. The size of cavities and aperture is estimated from the largest spheres which may fit them. (c) Possible tetravalent metal ions for preparing UiO-66 type MOFs. (d) Possible BDC type ligands for constructing UiO-66 type MOFs. Ligands labeled in blue indicate their corresponding MOFs have been reported. Reproduced from [28] and [29] with permissions, copyright American Chemical Society, 2015 and Royal Chemical Society, 2015.

membranes (MMMs) [30–84]. This review focuses on the study of polycrystalline UiO-66 membranes (shortened to UiO-66 membranes unless otherwise stated). However, their development was hindered. During the growth of UiO-66, the high charge density $Zr^{4+}$ polarizes the Zr-O bond to present covalent character, slowing down the ligand exchange rate [24]. In this case, it is unfavourable for defect repair during the crystallization process. Consequently, UiO-66 powders with poor crystallinity are harvested after a relatively long reaction time. Low nucleation density and poor intergrowth were reported in the fabrication of UiO-66 membranes.

The silence of the absence of dense UiO-66 membranes was broken by Liu et al. in 2015 [28]. After a thorough optimization of the preparation parameters (composition of mother solution, duration of synthesis and substrates), well-intergrown UiO-66 membrane was fabricated on $\alpha$-alumina hollow fibers and applied for water desalination. As stated by Liu et al. [28], high nucleation density of UiO-66 and satisfactory intergrowth could be achieved by adjusting the afore-mentioned preparation parameters. Water in the mother solution played an essential role [85], because the SBU of UiO-66 contains $OH^-$ ions in addition to $O^{2-}$ ions. Subsequently, a few continuous UiO-66 membranes supported on varying substrates were reported [86–89].

UiO-66 membranes were further developed by using modulated synthesis [59,90–96]. The so-called coordination modulation method was initially proposed by Tsuruoka et al. [97] and employed in UiO-66 crystal preparation by Schaate et al. [98]. Modulated synthesis of UiO-66 refers to regulating the coordination equilibrium by introducing modulators (e.g., formic or acetic or benzoic acid) as the organic ligands used to hinder the coordination interaction between $Zr^{4+}$ and BDC ligands [98]. As a result, the competitive reaction can adjust the rate of nucleation and crystal growth, improve the reproducibility of synthesis procedures and tune crystal features such as size, morphology, and crystallinity. That is in essence the reason why the fabrication of UiO-66 membranes benefited from modulated synthesis.

In this article, we review five approaches for preparing UiO-66 membranes and films, discuss their applications in gas, liquid and ion separations, and provide future perspectives on the development of their preparation methods and potential applications. Such a review about the specific MOF UiO-66 membranes aims to provide guidance for their in-depth investigation from basic research to practical application.

## 2 Approaches for fabricating UiO-66 membranes

Continuous growth of UiO-66 results in either a polycrystalline or an epitaxial film. As free-standing films were not mechanically robust, porous and nonporous substrates were employed to support UiO-66 membranes [28,59,86–96] and films [96,99–112], respectively. Porous metal and ceramic substrates with minimal permeation resistance in the configuration of flat sheets and tubes were adopted for supporting UiO-66 membranes. The main task for the synthesis of high-quality UiO-66 membranes is to control heterogeneous nucleation, crystallization and intergrowth on the substrate surface, and minimize the nonselective intercrystal pinholes. The quality of UiO-66 membranes is assessed in terms of crystal structure and morphology and separation capacities. A variety of synthesis methods have been explored for obtaining UiO-66 membranes and films, such as *in situ* synthesis, secondary synthesis, biphase synthesis, gas-phase deposition and electrochemical deposition (Tables 1 and 2). The synthesis of UiO-66 membranes can be analogous to that of other MOF membranes [16,17,19] and zeolite membranes [6,113], as they are all crystalline porous materials.

### 2.1 *In situ* synthesis

*In situ* synthesis is defined as when a porous substrate is immersed in the mother solution without any UiO-66 crystals previously attached to the surface. The nucleation, growth and intergrowth of UiO-66 crystals on the substrate all take place during a single fabrication step.

As exemplified by Liu et al. [86], UiO-66 polycrystalline membranes were fabricated on the prestructured yttria-stabilized zirconia hollow fibers (YSZ HF) by an *in situ* solvothermal approach via a thorough optimization of the heating duration, composition, and temperature of the synthetic mother solutions. As depicted in Fig. 2(a), after 2 h of heating, a very thin amorphous gel layer was formed on the top of the substrate. This was possibly caused by the aggregation of gel particles originating from the mother solution, which were transported to the substrate due to chemical interaction between the ligands and substrate, and Brownian motion. During the consequent synthesis, heterogeneous nucleation occurred probably at the interface of the gel and the solution (Fig. 2(a)), the only place where both the metal and ligand source were present in abundance. In parallel, further gel settlement could still be proceeding, which buried and disturbed the UiO-66 nuclei. Afterwards, crystals propagated through the gel network and then sank to the substrate by consuming the gel around them. Meanwhile, the aggregation and densification of nanocrystals occurred. With prolonged heating, crystal growth occurred (Fig. 2(a)) by acquisition of nutrients from the bulk solution, from nearby unreacted amorphous gel and small UiO-66 crystals (Ostwald ripening). A well-intergrown membrane layer (Fig. 2(a) and (c)) was finally fabricated after continuous heating for 48 h.

As stated by Liu et al. [86], since this membrane was fabricated with simultaneous growth and nucleation, UiO-66 crystals emerging on the surface of the membrane layer

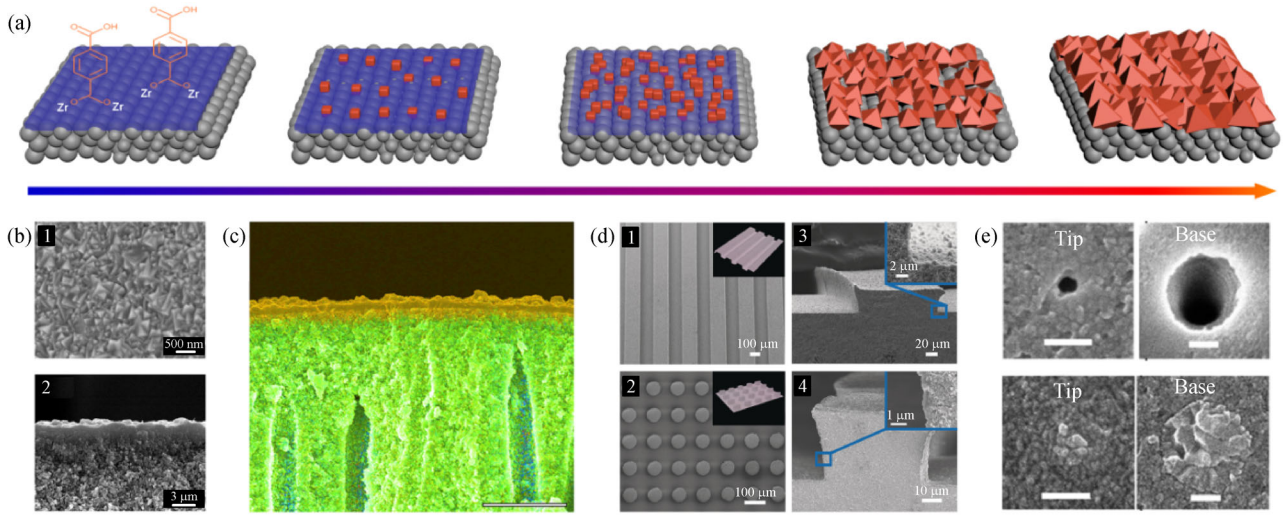


**Fig. 2** (a) Schematic diagram showing *in situ* synthesis of UiO-66 membranes on YSZ substrate. Scanning electron microscopy (SEM) images of UiO-66 membranes via *in situ* synthesis on $\alpha$-alumina hollow fibers (b), YSZ hollow fibers (c), EDXS mapping image, C signal, yellow; Y signal, green, micropatterned YSZ sheets (d) and nanochanneled PET films (scale bar 100 nm) (e). Reproduced from [28,86–88] with permissions, copyright John Wiley and Sons, 2017, 2018; American Chemical Society, 2015; the American Association for the Advancement of Science, 2018.

were identified in the EDX mapping image (Fig. 2(c)). FTIR-ATR characterization indicated that chemical bonds were established between the UiO-66 ligands and substrate, probably between the carboxyl and zirconium. This chemical interaction provides evidence for disclosing the energy-dispersive X-ray spectroscopy (EDXS) mapping (Fig. 2(c)). Although no visible UiO-66 crystals were found in the bulk substrate (Fig. 2(j)), slight intrusion of the C signal (yellow) into the substrate (green) was observed. This might be because the substrate was chemically modified by the BDC ligands during membrane preparation. The chemical interaction could boost the adhesion of the membrane layer to the substrate to a large extent, improving membrane stability.

Viability of the *in situ* synthesis of UiO-66 membranes was tested on varying substrates with different shape and roughness, for example, $\alpha$-alumina hollow fibers (Fig. 2 (b)) [28], micropatterned YSZ sheets (Fig. 2(d)) [87], and nanochanneled polyethylene terephthalate (PET) films (Fig. 2(e)) [88]. Apart from fabrication on bare substrates, modified substrates were adopted to facilitate membrane growth, such as $ZrO_2$ [90] and 3-aminopropy-ltriethoxysilane (APTES) modified $\alpha$-alumina tubes [89]. In addition, attempts were made to obtain UiO-66 films by *in situ* synthesis using bare $ZrO_2$ fibrous mats [101], and modified substrates including fluorine-doped tin oxide (FTO) glasses [99], polyurethane (PU) foams [100], polyacrylonitrile (PAN) fibers [102], silanized $\alpha$-alumina and ob-SiC foams [103].

## 2.2 Secondary growth

Secondary growth is defined as when a porous substrate is immersed in the mother solution with UiO-66 crystals previously attached to the surface. In comparison with the *in situ* synthesis, the nucleation and growth of polycrystalline membranes can be well-balanced by the secondary growth method.

Modulated synthesis was used in the case of secondary growth of UiO-66 membranes and films. Larger and isolated UiO-66 crystals were always produced with the addition of a modulator, whereas microsized intergrown UiO-66 crystals were yielded without modulation. The addition of monocarboxylic acid modulator could probably form complexes with zirconium cations [98]. Molecular zirconium complexes with different monocarboxylic acids ($HO_2CR$, R = *t*-Bu, $C(CH_3)_2Et$, etc.) [114,115] and structures similar to that of the SBU in UiO-66 have been described. Such complexes could act as intermediates and the framework construction would then proceed through an exchange between modulator and linker molecules at the coordination sites of the zirconium ion [98]. The application of modulators would decrease the possibility that the linker is connected to the SBU. Therefore, the formation of framework nuclei is disfavored, thus promoting the incubation of larger UiO-66 crystals. Furthermore, modulators can inhibit UiO-66 crystal growth in the (111) direction, leading to the formation of octahedral crystalline configurations rather than the cubic lattices generated from the original synthesis [27].

Friebe et al. [95] reported (002)-oriented UiO-66 membranes employing secondary growth with benzoic acid as a modulator. The growth started from randomly oriented seed crystals until they contacted each other. Afterwards, the crystals grew along the direction with the

highest growth rate (i.e., (002)), thus building the top layer of the membrane. The SEM top view in Fig. 3(a) shows the tips of the UiO-66 octahedrons, in good accordance with the model of the van der Drift growth [116]. The cross-section images reveal a 5 μm thick layer with a high orientation and the tilting angle of the octahedrons is around 15° (Fig. 3(a)).

Taking advantage of the uniform size and shape of the octahedral UiO-66 crystals, Lu et al. [117] produced large-area 2D oriented monolayers on a water surface through a liquid-air interfacial assembly technique (Fig. 3(b)). The obtained monolayers can be further transferred easily to a silicon platform and (111)-oriented UiO-66 films with long-range 3D superlattices can be formed (Fig. 3(b)). Furthermore, UiO-66 films with preferred (111) orientation were fabricated by repeated solvothermal synthesis (Fig. 3(c)) [105].

### 2.3 Biphase synthesis

As claimed in the modulated synthesis, isolated UiO-66 crystals were always produced instead of intergrown ones. An interpretation was provided by Shan et al. [96] that the partially deprotonated ligand caused by the accumulated protons in the reaction solution is the key factor preventing the intergrowth of the UiO-66 crystals (Fig. 4). With the addition of a deprotonating agent, trimethylamine (TEA), in an *in situ* biphase solvothermal reaction (Fig. 4), well-intergrown UiO-66 membranes and films were fabricated with tunable (200) and (111) orientations. As shown in

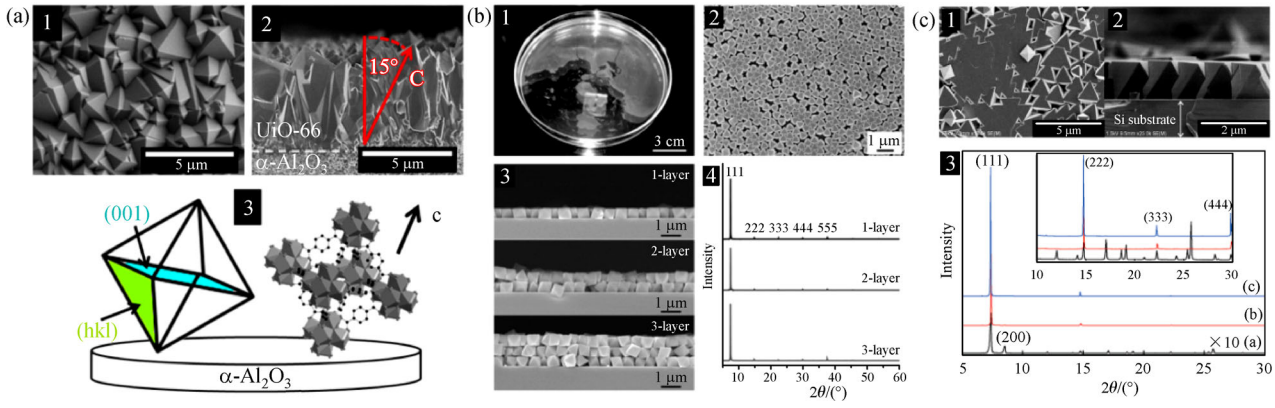


**Fig. 3** (a) SEM images ((1) surface; (2) cross section) of the UiO-66 membrane prepared by secondary growth and scheme (3) of the octahedrons' orientation within the UiO-66 membrane and their orientation to the substrate surface; (b) photograph (1) and SEM image (2) of 2D monolayer UiO-66 on a water surface and a silicon platform, respectively; cross-sectional SEM images (3) and the corresponding X-ray diffraction (XRD) patterns (4) of silicon platform-supported UiO-66 films comprising one, two, and three monolayers of microcrystals prepared by repetition of the transfer process using self-assembly; (c) SEM images (1) surface; (2) cross section) of UiO-66 film prepared by three repeated solvothermal syntheses and the corresponding XRD patterns (3). Reproduced from [95,105,117] with permissions, copyright American Chemical Society, 2017; John Wiley and Sons, 2013; Royal Chemical Society, 2015.

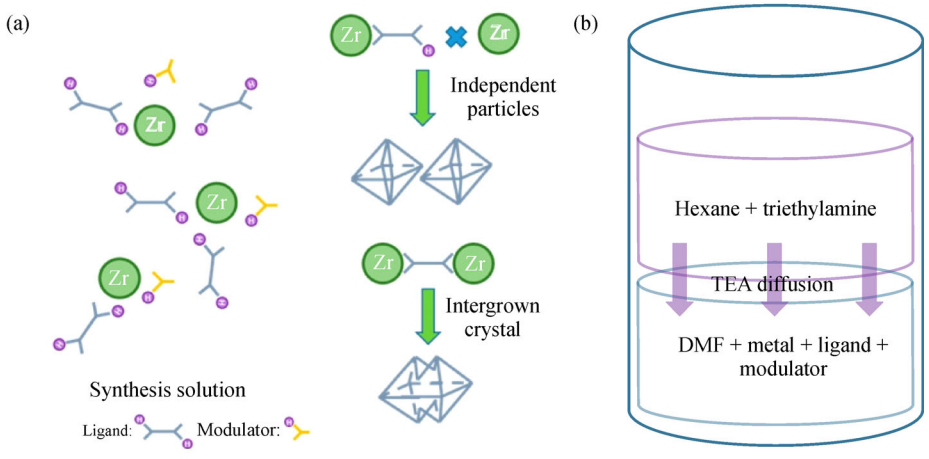


**Fig. 4** Schematic illustrations of (a) terminated and enabled intergrowth of UiO-66 crystals based on ligand deprotonation and (b) the biphase system to synthesize UiO-66 membranes and films. Reproduced from [96] with permission, copyright American Chemical Society, 2018.

Fig. 4(b), a hexane-dimethylformamide (DMF) biphase system was designed. TEA was initially dissolved in the hexane phase, and metal and ligand sources were charged in the DMF phase together with the modulator. Since the TEA could diffuse from the hexane phase to DMF phase and act as a deprotonating agent, the quantity of partially deprotonated ligands were efficiently reduced. Finally, the intergrowth between UiO-66 crystals was facilitated, affording dense membranes.

### 2.4 Gas-phase deposition

Atomic layer deposition (ALD) [118–122] in a mode also known as molecular layer deposition (MLD) is a technique where two or more precursors are individually pulsed into a reaction chamber in the gas phase and left to react with and saturate the surface of a substrate. When the surface is saturated by the first precursor, excess precursor is carried away by purging with an inert gas, and then the second precursor is applied in the same way. A thin-film is constructed with a thickness of one atomic layer or one molecular layer at a time by reiterating these steps in a cyclic process.

Lausund et al. [106] deposited UiO-66 thin films in an all-gas-phase process by the aid of ALD. Sequential reactions of $ZrCl_4$ and 1,4-benzenedicarboxylic acid formed amorphous organic–inorganic hybrid films that are crystallized to the UiO-66 structure after the treatment in acetic acid vapour (Fig. 5(a) and Table 2). The stoichiometry between metal clusters and organic linkers was well controlled by modulation of the ALD growth with additional acetic acid pulses. Unlike other fabrication methods, which rely on solvothermal nucleation and growth, the all-gas-phase method is based on scalable, solvent-free, seed-free, thickness-controllable, a well-established material processing technology to coat irregular substrates.

By applying vapor-assisted conversion (VAC) [108], highly oriented thin films of UiO-66 and UiO-66($NH_2$), were produced on a variety of surfaces — bare gold, gold surfaces modified with thiol SAMs, and bare silicon (Fig. 5(b)). The obtained MOF films are well intergrown and possess a high degree of crystallinity and crystal orientation extending to large areas. The relationship between the rate of crystallization and formation of the oriented MOF film was revealed by adjusting the parameters including modulator equivalents, precursor concentration, temperature, and reaction duration.

### 2.5 Electrochemical deposition

Electrochemical MOF deposition [123] has been proposed as a promising method for *in situ* deposition and patterning on conductive surfaces on the basis of two different

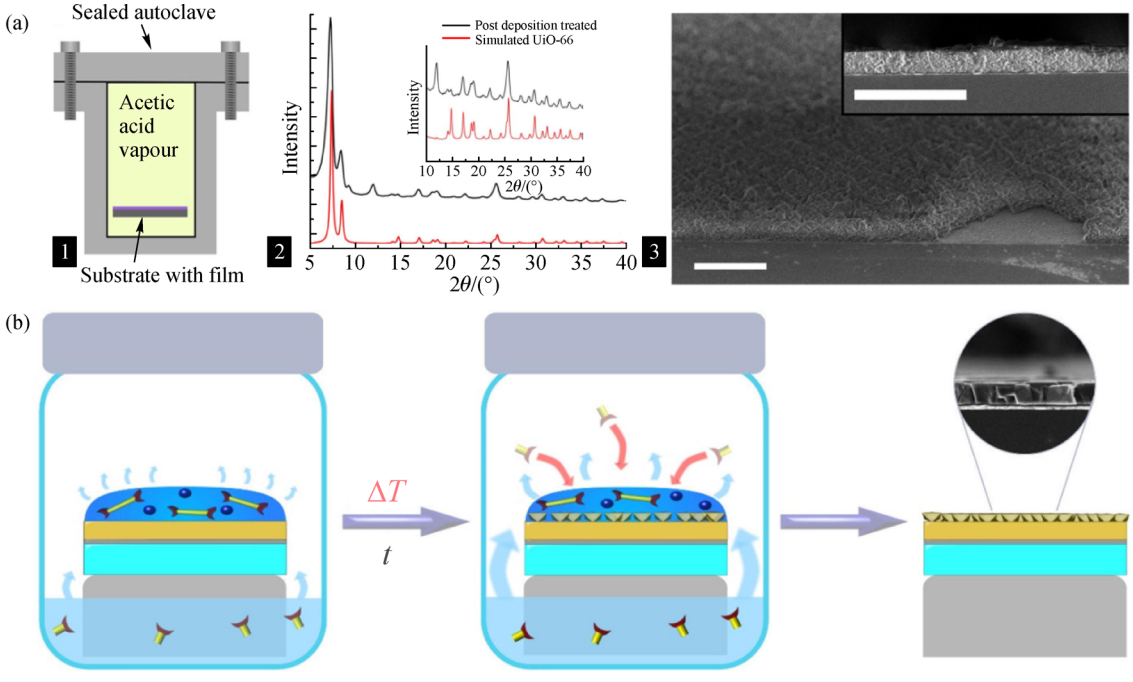


**Fig. 5** Fabrication of UiO-66 related films via gas-phase deposition. (a) Deposition of UiO-66 films by all-gas phase process: (1) experimental setup for post-treatment of the hybrid films with acetic acid vapor; XRD patterns (2) and cross-sectional SEM images (3) of the UiO-66 film after the treatment with acetic acid. (b) Schematic diagram of the vapor-assisted conversion process for the fabrication of (111)-oriented UiO-66-$NH_2$ films. $ZrOCl_2$, BDC-$NH_2$, and the modulator acetic acid (if desired) were dissolved in DMF giving the precursor solution on top of the substrate; a mixture of DMF and acetic acid giving the vapor source at the bottom of the vessel. Reproduced from [106,108] with permissions, copyright Springer Nature, 2016 and American Chemical Society, 2018.

mechanisms corresponding to anodic and cathodic deposition. In anodic deposition, MOF film formation occurs on a metal anode in contact with a ligand solution in virtue of the release of a critical concentration of metal ions by anodic dissolution [124]. On the other side (cathodic deposition), a solution containing metal ions, ligands, and a so-called probase is put in contact with a cathodic surface. Film deposition in this case relies on an increase in pH near the cathodic surface, where electrochemical reduction of the probase leads to local base generation and subsequent ligand deprotonation, enabling MOF formation [125].

As demonstrated by Stassen et al. [110], electrochemical deposition of the UiO-66 and its isoreticular analogues has been identified and elucidated. The crystallite size, film morphology, together with the deposition mechanism were rationalized through synthesis modulation. Whereas anodic deposition results in superior adhesion of the MOF layer onto the metallic zirconium substrate, which is attributed to the formation of an oxide bridging layer (Fig. 6), cathodic deposition has the merit of broad substrate flexibility.

Electrophoretic deposition (EPD) was used for the patterned growth of UiO-66 thin films on conductive glasses [109]. EPD is a well-established technique for depositing thin films, especially from nanoparticulate building blocks. The application of a DC electric field to a suspension composed of charged particles and nonpolar solvent can result in particle transport and deposition onto a conductive substrate [109]. During the synthesis of UiO-66, some surface defects are present (possibly due to missing metal nodes), which will give rise to partially negative charges on its surface. During the EPD process, those negative charges drive the particles toward the positively charged electrode and fabricate films.

## 3 Applications of UiO-66 membranes

Applications of UiO-66 membranes were predominately located in the separation field. The effective aperture size and functional groups of the UiO-66 type MOFs determine the membrane separation capability as predicted by molecular sieving and adsorption-diffusion mechanism. The flexibility of framework, missing ligand defects and substitutes on the ligands redefine the aperture size of UiO-66 rather than the 0.6 nm as estimated from crystallographic data. The functional groups of UiO-66 type MOFs are abundant. The OH groups from SBU, as well as the phenyl and the substituent groups from the ligands provide versatile adsorption sites. Herein, we discuss four categories of application based on membrane processes (Tables 1 and 2): gas separation, pervaporation, nanofiltration and electrochemical ion separation.

### 3.1 Gas separation

Liu et al. [28] applied the UiO-66 membranes constructed by *in situ* synthesis to gas separation. The gas permeance did not follow the kinetic diameters of the gases because of the larger aperture size of UiO-66 (~6.0 Å) (Fig. 7(a)). Figure 7(b) shows the kinetic diameters of the studied gases. The $H_2$ permeance was ca. $7.2\times 10^{-7}$ mol·m$^{-2}$·s$^{-1}$·Pa$^{-1}$, with a high $H_2/N_2$ ideal selectivity of 22.4. Owing to the effect of preferential $CO_2$ adsorption, the permeance of $CO_2$ ($9.5 \times 10^{-7}$ mol·m$^{-2}$·s$^{-1}$·Pa$^{-1}$) is higher than that of all the other studied gases, leading to a satisfactory $CO_2/N_2$ separating selectivity (29.7). As claimed, UiO-66 was a good membrane material for the purpose of $H_2$ purification and $CO_2$ capture. The similar order of gas permeation was recently confirmed by Wu et al. [126].

Gas separation was also performed by Friebe et al. [95] using (002) orientated UiO-66 membranes fabricated by secondary growth with modulated synthesis. Different from the above observation, the permeance of $CO_2$ was lower than that of $H_2$ and $N_2$ (Fig. 7(b)). The permeance of $H_2$ is the highest compared with that of the other gases ($N_2$, $CO_2$, $CH_4$, $C_2H_6$, $C_3H_8$), and the permeance decreased significantly with kinetic gas diameter, which seems to be

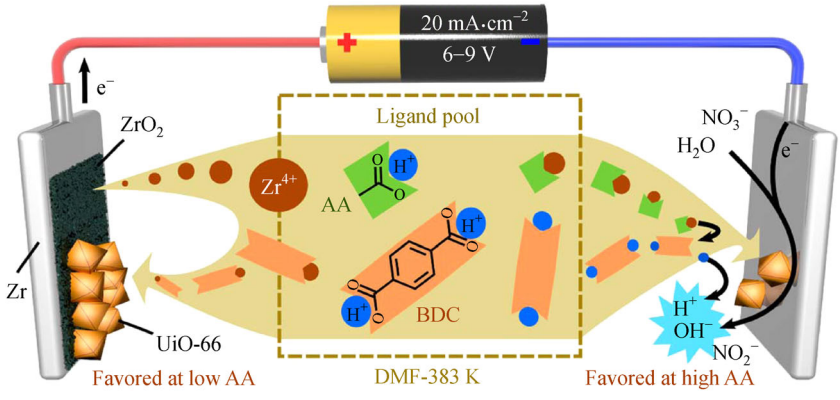


**Fig. 6** Schematic illustration of the anodic and cathodic electrochemical deposition mechanisms for UiO-66 films. Reproduced from [110] with permission, copyright American Chemical Society, 2015.

**Table 1** Summary of UiO-66 type membranes in terms of substrates, synthetic approaches and applications

| Materials | Substrates | Synthetic approaches | Applications | Ref. |
|---|---|---|---|---|
| UiO-66 | $\alpha$-Alumina hollow fibers | *In situ* synthesis ($Zr^{4+}$/BDC/$H_2O$/DMF = 1:1:1:500, 72 h, 120°C) | Nanofiltration ($K^+$, $Na^+$, $Ca^{2+}$, $Mg^{2+}$, $Al^{3+}$, $Cl^-$, $H_2O$) Gas separation ($H_2$, $CO_2$, $N_2$, $CH_4$) | [28] |
| UiO-66 | YSZ hollow fibers | *In situ* synthesis ($Zr^{4+}$/BDC/$H_2O$/DMF = 1:1:1:500, 48 h, 120°C) | Pervaporation (furfural, THF, acetone, *i*-butanol, *n*-butanol, propanol, ethanol, water) | [86] |
| UiO-66 | Micro-patterned YSZ discs | *In situ* synthesis ($Zr^{4+}$/BDC/$H_2O$/DMF = 1:1:1:500, 48 h, 120°C) | Pervaporation (*n*-butanol, water) | [87] |
| UiO-66 | Channeled PET | *In situ* synthesis ($Zr^{4+}$/BDC/DMF = 1:1:500, 24 h, 100°C) | Electro-chemical ion separation ($Li^+$, $Na^+$, $K^+$, $Rb^+$) | [88] |
| UiO-66-$NH_2$ | $ZrO_2$ modified alumina tubes | *In situ* synthesis (modified substrates) ($Zr^{4+}$/BDC-$NH_2$/$H_2O$/$CH_3COOH$/DMF = 1:1:1:150:500, 48 h, 120°C) | Pervaporation (thiophene, *n*-octane) | [90] |
| UiO-66-$NH_2$ | APTES modified $\alpha$-alumina tubes | *In situ* synthesis (modified substrates) ($Zr^{4+}$/BDC-$NH_2$/$H_2O$/DMF = 1:1:1:500, 24 h, 120°C) | Pervaporation ($Na^+$, $K^+$, $Ca^{2+}$, $Mg^{2+}$, $NH^{4+}$, $F^-$, $Cl^-$, and $NO^{3-}$, $H_2O$) | [89] |
| UiO-66 | $\alpha$-alumina tubes | Secondary growth ($Zr^{4+}$/BDC/$H_2O$/$CH_3COOH$/DMF = 1:1:1:500:*x*, *x* = 750, 1000, 1500, 24 h, 120°C, repeated three times) | Pervaporation (Methanol, ethanol, acetone, water, xylene, trimethylbenzene) Gas separation ($H_2$, $CO_2$, $N_2$) | [91] |
| UiO-66-$CH_3$ | Porous Ni sheets | Secondary growth ($Zr^{4+}$/BDC-$CH_3$/$CH_3COOH$/DMF = 1:1:30:430, 24 h, 120°C) | Gas separation ($CO_2$, $N_2$) | [92] |
| UiO-66 | $\alpha$-Alumina tubes | Secondary growth ($Zr^{4+}$/BDC-$NH_2$/$H_2O$/$CH_3COOH$/DMF = 1:1:1:150:500, 72 h, 120°C) | Pervaporation (methanol, methyl *tert*-butyl ether) | [93] |
| UiO-66-$(OH)_2$ | $\alpha$-Alumina hollow fibers | Secondary growth ($Zr^{4+}$/ODBDC/HCOOH/DMF = 1:1:100:500, 72 h, 120°C) | Nanofiltration ($Fe^{3+}$, $Cr^{3+}$, $Zn^{2+}$, $Mg^{2+}$, $Na^+$, $Cl^-$, $H_3BO_3$, methyl blue, $H_2O$) | [94] |
| UiO-66 | $\alpha$-Alumina discs | Secondary growth ($Zr^{4+}$/BDC/Benzoic acid/DMF = 1:1:20:100, 24 h, 180°C) | Gas separation ($H_2$, $CO_2$, $N_2$, $CH_4$, $C_2H_6$, $C_3H_8$) | [59,95] |
| UiO-66 | Anodic aluminum oxide, AAO | Secondary growth ($Zr^{4+}$/BDC/$H_2O$/DMF = 1:1:1:500, 72 h, 120°C) | Gas separation ($H_2$, $CO_2$, $N_2$, $CH_4$) | [126] |
| UiO-66 | $\alpha$-Alumina discs | Biphase synthesis DMF phase: 15 mL, Zr/BDC/HCOOH/DMF = 1:0.5:125:130, and 1:0.7:125:130, Hexane phase: 1836 mg TEA in 15 mL hexane, 24 h, 120°C | Gas separation ($CO_2$, $N_2$) | [96] |

**Table 2** Summary of UiO-66 films in terms of substrates, synthetic approaches and applications

| Materials | Substrates | Synthetic approaches | Applications | Ref. |
|---|---|---|---|---|
| UiO-66 | BDC functionalized FTO glasses | *In situ* synthesis (modified substrate) ($Zr^{4+}$/BDC/$CH_3COOH$/DMF = 1:1:96:520, 24 h, 120°C) | Cyclic voltammetry ion separation ($Ru(NH_3)_6^{3+}$, $Fe(phen)_3^{2+}$, $Fe(CN)_6^{3+}$) | [99] |
| UiO-66-$SO_3H$-$NH_2$ | PDA-coated PU foams | *In situ* synthesis (modified substrate) ($Zr^{4+}$/BDC-$SO_3H$/BDC-$NH_2$/$H_2O$/$CH_3COOH$ = 1:0.75:0.25:230:100) | Catalysis (from glucose to HMF) | [100] |
| UiO-66 | $ZrO_2$ fibrous mats | *In situ* synthesis ($ZrO_2$/BDC/$CH_3COOH$/$H_2O$ = 1:3.7:2.2:686) | Not reported | [101] |
| UiO-66-$NH_2$ | ATA modified PAN fibers | *In situ* synthesis (modified substrate) ($Zr^{4+}$/BDC-$NH_2$/acetone = 1:1:200) | Chlorine adsorption | [102] |
| UiO-66 | Silanized $\alpha$-alumina and ob-SiC foams | *In situ* synthesis (modified substrate) ($Zr^{4+}$/BDC//DMF = 1:0.9:380, 24 h, 120°C) | Not reported | [103] |
| UiO-66 | Stainless meshes | Secondary growth (Zirconium propoxide/BDC/DMF, 12 h, RT) | Oil-water separation (diesel, vegetable oil, pump oil, cyclohexane, water) | [104] |
| UiO-66 | Si discs | Secondary growth ($Zr^{4+}$/BDC/$H_2O$/$CH_3COOH$/DMF = 1:1:1:0/500:1500, 24 h, 120°C, repeated three times) | Not reported | [105] |
| UiO-66 | Si discs | Gas-phase deposition ($ZrCl_4$ (165°C), BDC (220°C), $CH_3COOH$ (RT), $N_2$; post treatment: 160°C $CH_3COOH$, 24 h) | Not reported | [106] |
| UiO-66-$NH_2$ | Si discs | Gas-phase deposition ($ZrCl_4$ (165°C), BDC-$NH_2$ (225°C), $N_2$; post treatment: 160°C $CH_3COOH$, 24 h) | Not reported | [107] |
| UiO-66-$NH_2$ (UiO-66) | Gold, Si discs | Vapor-assistant conversion (Precursor solution: $ZrOCl_2 \cdot 8H_2O$ + BDC-$NH_2$ (BDC) + $CH_3COOH$ + DMF Vapor source: DMF + $CH_3COOH$, 100°C, 3 h) | Ethanol adsorption | [108] |
| UiO-66 | FTO glasses | Electrophoretic deposition (10 mg UiO-66 particles in 20 mL toluene, DC voltage of 90 V) | Not reported | [109] |
| UiO-66 | Zirconium foil | Electrochemical deposition (BDC:$HNO_3$:$H_2O$:$CH_3COOH$:DMF = 1:2:4:5/10/50:130, 80 mA, 110°C) | Sorbent trap (Toluene) | [110] |
| UiO-66 | Free-standing | Biphase synthesis DMF phase: 5 mL, Zr/BDC/HCOOH/DMF = 1:0.25:87.5:130, 1:0.25:100:130, 1:0.25:118:130, 1:0.4:125:130, 1:0.5:125:130, 1:0.7:125:130, 1:0.6:150:130, 1:0.84:150:130 Hexane phase: 612 mg TEA in 5 mL hexane, 120°C, 24 h | Not reported | [96] |
| UiO-66 | Cellulose supports | Filtration (UiO-66 particles in water) | Nanofiltration (methylene blue, water) | [111] |
| UiO-66 | Silicon wafers | Solution shearing (UiO-66 particles in DMF/$H_2O$/MeOH) | Not reported | [112] |
| UiO-66 | Silicon platform | Self-assembly (PVP modified UiO-66 in ethanol/water solution containing sodium dodecyl sulfate) | Not reported | [117] |

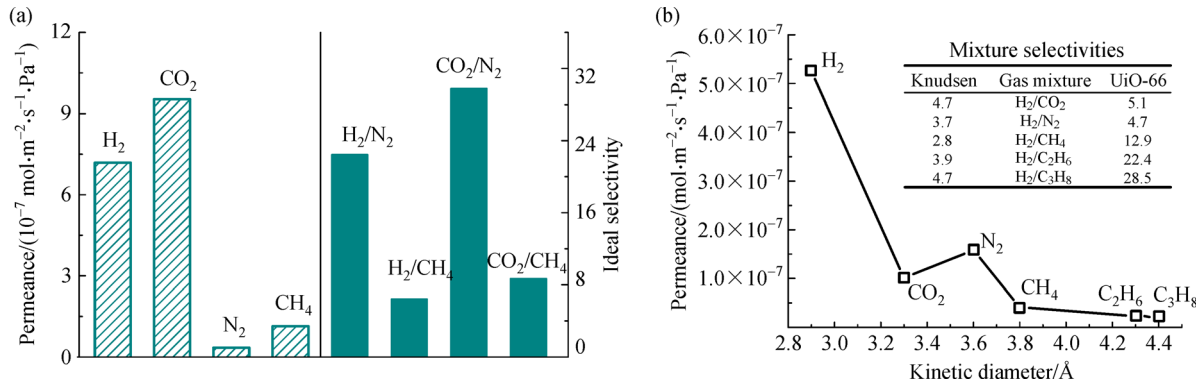


**Fig. 7** (a) Single component permeation data of UiO-66 membranes at 293 K with 1 bar pressure difference; (b) $H_2$ mixed binary permeation data of (002) oriented UiO-66 membrane at 298 K and 1 bar (absolute pressure) in both feed and sweep sides. Reproduced from [28,95] with permissions, copyright American Chemical Society, 2015 and 2017.

in good accordance with the concept of molecular sieving. The selectivity of $H_2/C_3H_8$ reached the highest, being 28.5. Furthermore, the gas separation performance of UiO-66 type membranes was investigated by Liu et al. [92], Miyamoto et al. [91] and Shan et al. [96].

### 3.2 Pervaporation

In 2017, Liu et al. [28] reported UiO-66 membranes for organic dehydration. The membrane was activated on-stream and remained robust after being treated with boiling benzene and water. No discernible degradation of membrane performance was recognized in the following 200 hours' stability test for water/*n*-butanol and water/furfural separation even sulfuric acid was introduced (Fig. 8(a)). At higher temperature (e.g., 80°C), the membranes exhibited a very high flux of up to ca. 6.0 kg·m$^{-2}$·h$^{-1}$ and great separation factor ( > 45000). This performance, in terms of separation factor, is 10–100 times of commercially available silica and polymeric membranes with equivalent flux. The resistance against harsh environments was superior to commercial zeolite NaA membranes. Under the same *in situ* synthesis condition, Huang et al. [87] fabricated UiO-66 membranes on micropatterned YSZ substrates. The resulting membranes displayed a 100% improvement in the apparent water permeation flux over conventional flat UiO-66 membranes without compromising the separation factor of water over *n*-butanol.

Wu et al. [90] synthesized UiO-66-$NH_2$ membranes for pervaporative desulfurization with an optimum permeation flux of 2.16 kg·m$^{-2}$·h$^{-1}$ and a separation factor of 17.86 under 40°C for 1312 ppm thiophene/*n*-octane mixtures. The separation factor is higher than polymer-based membranes in the literature (Fig. 8(b)). As evidenced, the preferential adsorption of thiophene is an important contribution to the selectivity. Moreover, the studies from Wan et al. [89], Miyamoto et al. [91] and Wu et al. [93] extended the applications of pervaporation to other systems.

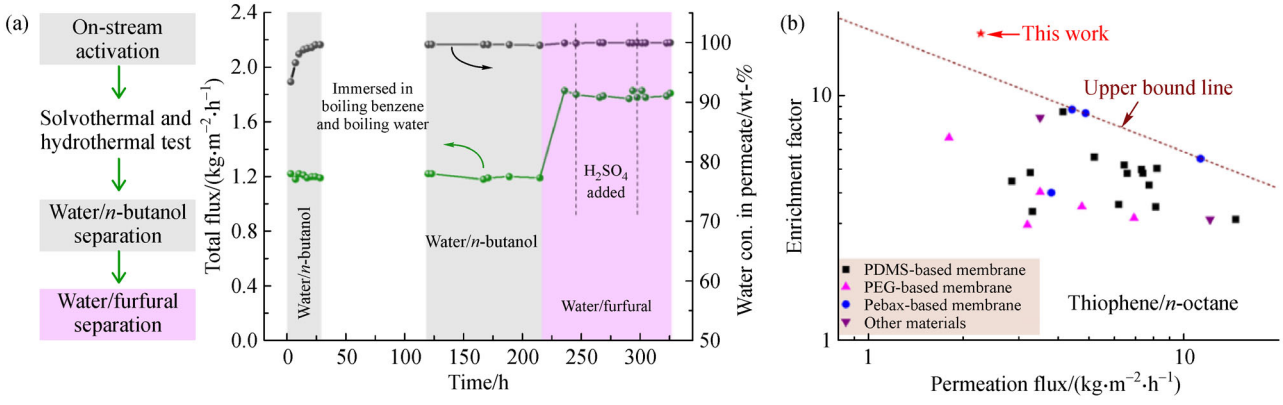


**Fig. 8** (a) Flow chart and pervaporative organic (*n*-butanol and furfural) dehydration performance of UiO-66 membranes during on-stream activation and stability test processes at 30°C with 5 wt-% water in the feed; (b) thiophene/*n*-octane separation performance of UiO-66-$NH_2$ membrane and a comparison with polymers. Reproduced from [86,90] with permissions, copyright John Wiley and Sons, 2017, and Elsevier, 2018.

### 3.3 Nanofiltration

UiO-66 membranes were applied in water-softening for multivalent and trivalent cations rejection (86.3%, 98.0%, and 99.3% for $Ca^{2+}$ (0.82 nm), $Mg^{2+}$ (0.86 nm), and $Al^{3+}$ (0.95 nm), respectively) in light of the size exclusion effect (Fig. 9(a)) [28]. Although the diameter of hydrated monovalent ions ($Cl^-$: 0.66 nm, $K^+$: 0.66 nm, and $Na^+$: 0.72 nm) exceeded the aperture size of UiO-66 (~6.0 Å), the rejections were moderate (i.e., 45.7% and 47.0% for $K^+$ and $Na^+$, respectively). Two possible reasons were proposed: one is the ligand dynamics of UiO-66 [127] because its carboxylate groups can change their coordination mode from edge-bridging to monodentate; the other is the missing-ligand defects [128–130] in the UiO-66 crystals.

Wang et al. [94] mitigated the ligand-missing defects in UiO-66(Zr)-$(OH)_2$ membranes by postsynthetic defect healing (PSDH), boosting the $Na^+$ rejection rate by 74.9% (from 26% to 45%), and achieved a perfect block of methyl blue (from 98.7% to 99.8%) (Figs. 9(b) and 9(c)). As anticipated, the membranes display excellent hydrothermal stability in aqueous solutions ( > 600 h).

### 3.4 Electrochemical ion separation

Zhang et al. [88] reported UiO-66 membranes for ultrafast selective transport of alkali metal ions. The resulting membranes can preferentially transport $Li^+$ over other alkali metal ions following unhydrated size exclusion mechanism, with the ion transport rate order of $Li^+ > Na^+ > K^+ > Rb^+$. The LiCl/RbCl selectivity is of ~1.8, which outperforms the LiCl/RbCl selectivity of 0.6–0.8 evaluated in traditional membranes (Fig. 10(a)). This study may potentially open up a new avenue for efficient ion separations in the future.

Cyclic voltammetry (CV) experiments were conducted to assess the molecular sieving capability of UiO-66 films supported on FTO using redox-active species (including $Ru(NH_3)_6^{3+}$ (diameter ca. 0.55 nm) and $Fe(phen)_3^{2+}$ (diameter ca. 1.3 nm)) as probes [99]. The UiO-66 coated electrodes showed moderate CV signals for $Ru(NH_3)_6^{3+}$ but were not responsive to $Fe(phen)_3^{2+}$, verifying their size-selective accessibility to these two species, which is in line with the fact that the pore aperture of UiO-66 (0.60 nm, estimated from crystallographic data) is between the diameter of $Ru(NH_3)_6^{3+}$ and $Fe(phen)_3^{2+}$. The ion discrimination of UiO-66 film (healing with polydimethylsiloxane (PDMS)) was further evidenced by the electrochemical study in a mixed solution of $Ru(NH_3)_6^{3+}$ and $Fe(phen)_3^{2+}$, where well-defined redox peaks were observed only for the former species (Fig. 10(b)).

## 4 Conclusions, remarks and perspectives

With adequate members of the UiO-66 family and exceptionally high stability, UiO-66 based membranes stand out from MOF membranes as well as novel porous material membranes for organic purification under harsh conditions.

Regarding synthetic protocols, *in situ* synthesis is a facile method for fabricating UiO-66 membranes. Electrochemical deposition will be a promising method for coating the membranes on devices. Although secondary growth is the benchmark method for large-scale production of polycrystalline zeolite membranes, gas assistant deposition [119] and interfacial synthesis [131] may have opportunities in scaled-up synthesis of UiO-66 membranes.

Precise separation is one of the future directions for membrane-based separation. The author speculates that there would be some optimal preparation conditions where the UiO-66 membranes have the opportunity for (i) separating isomers of hydrocarbons; furthermore, (ii) purification of organics under harsh conditions may offer the other position for UiO-66 membranes.

New membrane materials are always accompanied by

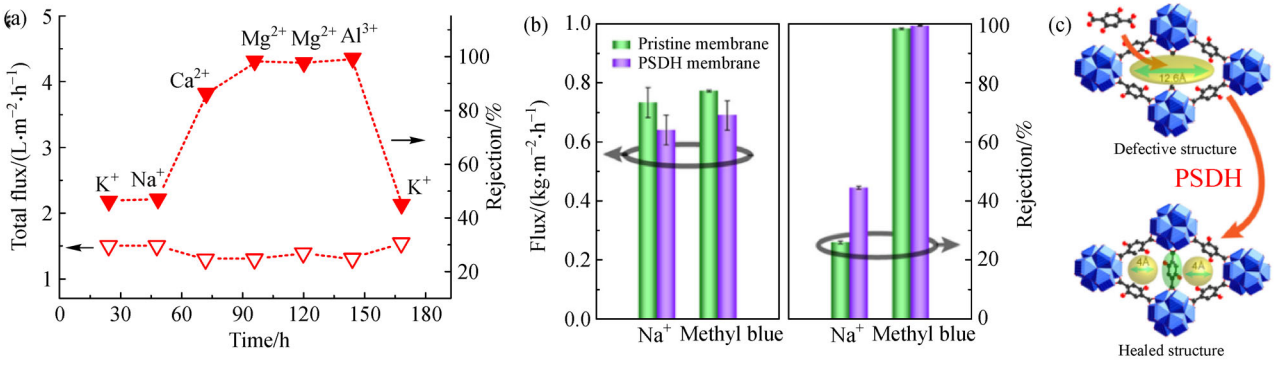


**Fig. 9** (a) Desalination performance of the UiO-66 membrane for KCl, NaCl, $CaCl_2$, $MgCl_2$ and $AlCl_3$ aqueous solutions with a concentration of 0.20 wt-% at 20°C under a pressure difference of 10.0 bar; (b) separation performance of the UiO-66-$(OH)_2$ membrane before and after PSDH under a pressure difference of 3 bar with 2000 ppm NaCl and 100 ppm methyl blue aqueous solutions; (c) scheme of PSDH by relinking. Reproduced from [28,94] with permissions, copyright American Chemical Society, 2015 and 2017.

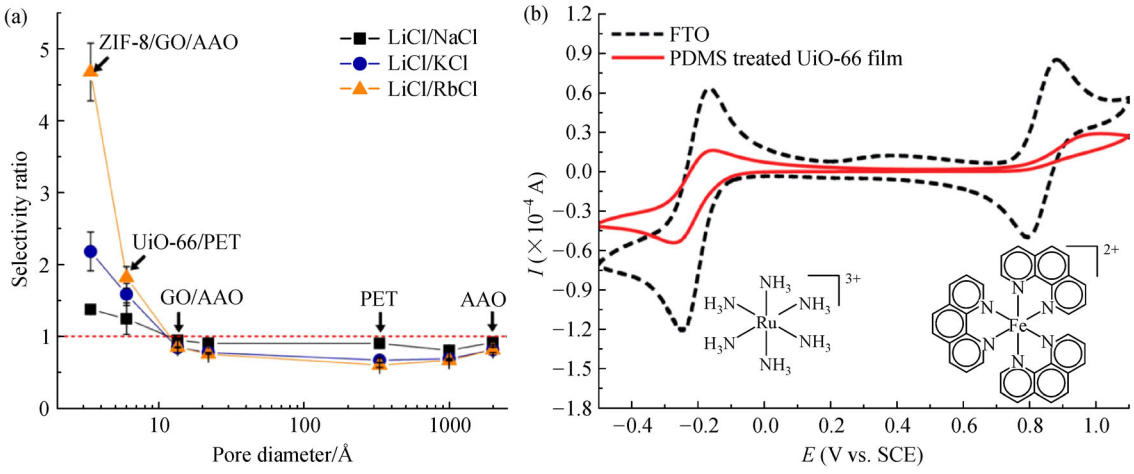


**Fig. 10** (a) Ion selectivity over the pore diameter of MOF and porous membranes; (b) cyclic voltammograms of $Ru(NH_3)_6^{3+}$/$Fe(phen)_3^{2+}$ mixture in aqueous solutions on MOF-coated electrode treated with PDMS (red solid lines) and bare FTO electrode (black dashed lines). Reproduced from [88,99] with permissions, copyright American Association for the Advancement of Science, 2018, and John Wiley and Sons, 2016.

challenges. (i) In line with the principle of green chemistry, water [132,133] is more welcome than DMF as an alternative solvent, which reduces the cost of UiO-66 membranes. Consequently, systemic optimization of synthetic variables is required. (ii) Novel zirconium sources are desired because the usual metal source $ZrCl_4$ requires careful storage to avoid deliquescence. (iii) Scalable synthesis requires a clear understanding of the membrane reproducibility and substrates.



## References

1. Park H B, Kamcev J, Robeson L M, Elimelech M, Freeman B D. Maximizing the right stuff: The trade-off between membrane permeability and selectivity. Science, 2017, 356(6343): eaab0530
2. Shan M, Liu X, Wang X, Yarulina I, Seoane B, Kapteijn F, Gascon J. Facile manufacture of porous organic framework membranes for precombustion $CO_2$ capture. Science Advances, 2018, 4(9): eaau1698
3. Liu X L, Li Y S, Zhu G Q, Ban Y J, Xu L Y, Yang W S. An organophilic pervaporation membrane derived from metal-organic framework nanoparticles for efficient recovery of bio-alcohols. Angewandte Chemie International Edition, 2011, 50(45): 10636–10639
4. Bernardo P, Drioli E, Golemme G. Membrane gas separation: A review/state of the art. Industrial & Engineering Chemistry Research, 2009, 48(10): 4638–4663
5. Lee K P, Arnot T C, Mattia D. A review of reverse osmosis membrane materials for desalination—Development to date and future potential. Journal of Membrane Science, 2011, 370(1): 1–22
6. Rangnekar N, Mittal N, Elyassi B, Caro J, Tsapatsis M. Zeolite membranes—a review and comparison with MOFs. Chemical Society Reviews, 2015, 44(20): 7128–7154
7. Furukawa H, Cordova K E, O'Keeffe M, Yaghi O M. The chemistry and applications of metal-organic frameworks. Science, 2013, 341(6149): 1230444
8. Arnold M, Kortunov P, Jones D J, Nedellec Y, Kärger J, Caro J. Oriented crystallisation on supports and anisotropic mass transport of the metal-organic framework manganese formate. European Journal of Inorganic Chemistry, 2007, 2007(1): 60–64
9. Gascon J, Aguado S, Kapteijn F. Manufacture of dense coatings of $Cu_3(BTC)_2$ (HKUST-1) on $\alpha$-alumina. Microporous and Mesoporous Materials, 2008, 113(1): 132–138
10. Liu Y, Ng Z, Khan E A, Jeong H K, Ching C, Lai Z. Synthesis of continuous MOF-5 membranes on porous $\alpha$-alumina substrates. Microporous and Mesoporous Materials, 2009, 118(1): 296–301
11. Yoo Y, Lai Z, Jeong H K. Fabrication of MOF-5 membranes using microwave-induced rapid seeding and solvothermal secondary growth. Microporous and Mesoporous Materials, 2009, 123(1): 100–106
12. Guo H, Zhu G, Hewitt I J, Qiu S. "Twin Copper Source" growth of metal-organic framework membrane: $Cu_3(BTC)_2$ with high permeability and selectivity for recycling $H_2$. Journal of the American Chemical Society, 2009, 131(5): 1646–1647
13. Ranjan R, Tsapatsis M. Microporous metal organic framework membrane on porous support using the seeded growth method. Chemistry of Materials, 2009, 21(20): 4920–4924

14. Bux H, Liang F, Li Y, Cravillon J, Wiebcke M, Caro J. Zeolitic imidazolate framework membrane with molecular sieving properties by microwave-assisted solvothermal synthesis. Journal of the American Chemical Society, 2009, 131(44): 16000–16001
15. Venna S R, Carreon M A. Highly permeable zeolite imidazolate framework-8 membranes for $CO_2/CH_4$ separation. Journal of the American Chemical Society, 2010, 132(1): 76–78
16. Qiu S, Xue M, Zhu G. Metal-organic framework membranes: From synthesis to separation application. Chemical Society Reviews, 2014, 43(16): 6116–6140
17. Yao J, Wang H. Zeolitic imidazolate framework composite membranes and thin films: Synthesis and applications. Chemical Society Reviews, 2014, 43(13): 4470–4493
18. Li X, Liu Y, Wang J, Gascon J, Li J, Van der Bruggen B. Metal-organic frameworks based membranes for liquid separation. Chemical Society Reviews, 2017, 46(23): 7124–7144
19. Liu Y, Ban Y, Yang W. Microstructural engineering and architectural design of metal-organic framework membranes. Advanced Materials, 2017, 29(31): 1606949
20. Peng Y, Li Y, Ban Y, Jin H, Jiao W, Liu X, Yang W. Metal-organic framework nanosheets as building blocks for molecular sieving membranes. Science, 2014, 346(6215): 1356–1359
21. Liu Y, Pan J H, Wang N, Steinbach F, Liu X, Caro J. Remarkably enhanced gas separation by partial self-conversion of a laminated membrane to metal-organic frameworks. Angewandte Chemie International Edition, 2015, 54(10): 3028–3032
22. Duan J, Jin W, Kitagawa S. Water-resistant porous coordination polymers for gas separation. Coordination Chemistry Reviews, 2017, 332: 48–74
23. Wang C, Liu X, Keser Demir N, Chen J P, Li K. Applications of water stable metal-organic frameworks. Chemical Society Reviews, 2016, 45(18): 5107–5134
24. Bai Y, Dou Y, Xie L H, Rutledge W, Li J R, Zhou H C. Zr-based metal-organic frameworks: Design, synthesis, structure, and applications. Chemical Society Reviews, 2016, 45(8): 2327–2367
25. Pearson R G. Hard and soft acids and bases. Journal of the American Chemical Society, 1963, 85(22): 3533–3539
26. Yuan S, Qin J S, Lollar C T, Zhou H C. Stable metal-organic frameworks with group 4 metals: Current status and trends. ACS Central Science, 2018, 4(4): 440–450
27. Cavka J H, Jakobsen S, Olsbye U, Guillou N, Lamberti C, Bordiga S, Lillerud K P. A new zirconium inorganic building brick forming metal organic frameworks with exceptional stability. Journal of the American Chemical Society, 2008, 130(42): 13850–13851
28. Liu X, Demir N K, Wu Z, Li K. Highly water-stable zirconium metal-organic framework UiO-66 membranes supported on alumina hollow fibers for desalination. Journal of the American Chemical Society, 2015, 137(22): 6999–7002
29. Hu Z, Zhao D. De facto methodologies toward the synthesis and scale-up production of UiO-66-type metal-organic frameworks and membrane materials. Dalton Transactions (Cambridge, England), 2015, 44(44): 19018–19040
30. Xu R, Wang Z, Wang M, Qiao Z, Wang J. High nanoparticles loadings mixed matrix membranes via chemical bridging-cross-linking for $CO_2$ separation. Journal of Membrane Science, 2019, 573: 455–464
31. Shen J, Liu G, Huang K, Li Q, Guan K, Li Y, Jin W. UiO-66-polyether block amide mixed matrix membranes for $CO_2$ separation. Journal of Membrane Science, 2016, 513: 155–165
32. Ghalei B, Sakurai K, Kinoshita Y, Wakimoto K, Isfahani Ali P, Song Q, Doitomi K, Furukawa S, Hirao H, Kusuda H, et al. Enhanced selectivity in mixed matrix membranes for $CO_2$ capture through efficient dispersion of amine-functionalized MOF nanoparticles. Nature Energy, 2017, 2(7): 17086
33. Liu L, Xie X, Qi S, Li R, Zhang X, Song X, Gao C. Thin film nanocomposite reverse osmosis membrane incorporated with UiO-66 nanoparticles for enhanced boron removal. Journal of Membrane Science, 2019, 580: 101–109
34. Pang J, Kang Z, Wang R, Xu B, Nie X, Fan L, Zhang F, Du X, Feng S, Sun D. Exploring the sandwich antibacterial membranes based on UiO-66/graphene oxide for forward osmosis performance. Carbon, 2019, 144: 321–332
35. Wang Y, Li X, Zhao S, Fang Z, Ng D, Xie C, Wang H, Xie Z. Thin-film composite membrane with interlayer decorated metal-organic framework UiO-66 toward enhanced forward osmosis performance. Industrial & Engineering Chemistry Research, 2019, 58(1): 195–206
36. Liu T Y, Yuan H G, Liu Y Y, Ren D, Su Y C, Wang X. Metal-organic framework nanocomposite thin films with interfacial bindings and self-standing robustness for high water flux and enhanced ion selectivity. ACS Nano, 2018, 12(9): 9253–9265
37. Prasetya N, Donose B C, Ladewig B P. A new and highly robust light-responsive Azo-UiO-66 for highly selective and low energy post-combustion $CO_2$ capture and its application in a mixed matrix membrane for $CO_2/N_2$ separation. Journal of Materials Chemistry. A, Materials for Energy and Sustainability, 2018, 6(34): 16390–16402
38. Ma L, Svec F, Tan T, Lv Y. Mixed matrix membrane based on cross-linked poly[(ethylene glycol) methacrylate] and metal-organic framework for efficient separation of carbon dioxide and methane. ACS Applied Nano Materials, 2018, 1(6): 2808–2818
39. Jia M, Feng Y, Qiu J, Zhang X F, Yao J. Amine-functionalized MOFs@GO as filler in mixed matrix membrane for selective $CO_2$ separation. Separation and Purification Technology, 2019, 213: 63–69
40. Gao Z F, Feng Y, Ma D, Chung T S. Vapor-phase crosslinked mixed matrix membranes with UiO-66-$NH_2$ for organic solvent nanofiltration. Journal of Membrane Science, 2019, 574: 124–135
41. Jiang Y, Liu C, Caro J, Huang A. A new UiO-66-$NH_2$ based mixed-matrix membranes with high $CO_2/CH_4$ separation performance. Microporous and Mesoporous Materials, 2019, 274: 203–211
42. Sánchez-Laínez J, Gracia-Guillén I, Zornoza B, Téllez C, Coronas J. Thin supported MOF based mixed matrix membranes of Pebax® 1657 for biogas upgrade. New Journal of Chemistry, 2019, 43(1): 312–319
43. Zhang X F, Feng Y, Wang Z, Jia M, Yao J. Fabrication of cellulose nanofibrils/UiO-66-$NH_2$ composite membrane for $CO_2/N_2$ separation. Journal of Membrane Science, 2018, 568: 10–16
44. Satheeshkumar C, Yu H J, Park H, Kim M, Lee J S, Seo M. Thiol-ene photopolymerization of vinyl-functionalized metal-organic

frameworks towards mixed-matrix membranes. Journal of Materials Chemistry. A, Materials for Energy and Sustainability, 2018, 6 (44): 21961–21968

45. Jiang X, Li S, He S, Bai Y, Shao L. Interface manipulation of $CO_2$-philic composite membranes containing designed UiO-66 derivatives towards highly efficient $CO_2$ capture. Journal of Materials Chemistry. A, Materials for Energy and Sustainability, 2018, 6(31): 15064–15073
46. Golpour M, Pakizeh M. Preparation and characterization of new PA-MOF/PPSU-GO membrane for the separation of KHI from water. Chemical Engineering Journal, 2018, 345: 221–232
47. Marti A M, Venna S R, Roth E A, Culp J T, Hopkinson D P. Simple fabrication method for mixed matrix membranes with *in situ* MOF growth for gas separation. ACS Applied Materials & Interfaces, 2018, 10(29): 24784–24790
48. Ahmad M Z, Navarro M, Lhotka M, Zornoza B, Téllez C, de Vos W M, Benes N E, Konnertz N M, Visser T, Semino R, et al. Enhanced gas separation performance of 6FDA-DAM based mixed matrix membranes by incorporating MOF UiO-66 and its derivatives. Journal of Membrane Science, 2018, 558: 64–77
49. Mozafari M, Abedini R, Rahimpour A. Zr-MOFs-incorporated thin film nanocomposite Pebax 1657 membranes dip-coated on polymethylpentyne layer for efficient separation of $CO_2/CH_4$. Journal of Materials Chemistry. A, Materials for Energy and Sustainability, 2018, 6(26): 12380–12392
50. Xiang F, Marti A M, Hopkinson D P. Layer-by-layer assembled polymer/MOF membrane for $H_2/CO_2$ separation. Journal of Membrane Science, 2018, 556: 146–153
51. Xu Y M, Japip S, Chung T S. Mixed matrix membranes with nano-sized functional UiO-66-type MOFs embedded in 6FDA-HAB/DABA polyimide for dehydration of C1–C3 alcohols via pervaporation. Journal of Membrane Science, 2018, 549: 217–226
52. Molavi H, Shojaei A, Mousavi S A. Improving mixed-matrix membrane performance via PMMA grafting from functionalized $NH_2$–UiO-66. Journal of Materials Chemistry. A, Materials for Energy and Sustainability, 2018, 6(6): 2775–2791
53. Zamidi Ahmad M, Navarro M, Lhotka M, Zornoza B, Téllez C, Fila V, Coronas J. Enhancement of $CO_2/CH_4$ separation performances of 6FDA-based co-polyimides mixed matrix membranes embedded with UiO-66 nanoparticles. Separation and Purification Technology, 2018, 192: 465–474
54. Rodrigues M A, Ribeiro J S, Costa E S, Miranda J L, Ferraz H C. Nanostructured membranes containing UiO-66 (Zr) and MIL-101 (Cr) for $O_2/N_2$ and $CO_2/N_2$ separation. Separation and Purification Technology, 2018, 192: 491–500
55. Sutrisna P D, Hou J, Zulkifli M Y, Li H, Zhang Y, Liang W, D'Alessandro Deanna M, Chen V. Surface functionalized UiO-66/Pebax-based ultrathin composite hollow fiber gas separation membranes. Journal of Materials Chemistry. A, Materials for Energy and Sustainability, 2018, 6(3): 918–931
56. Liu S, Sang X, Wang L, Zhang J, Song J, Han B. Incorporation of metal-organic framework in polymer membrane enhances vanadium flow battery performance. Electrochimica Acta, 2017, 257: 243–249
57. Donnadio A, Narducci R, Casciola M, Marmottini F, D'Amato R, Jazestani M, Chiniforoshan H, Costantino F. Mixed membrane matrices based on Nafion/UiO-66/$SO_3$H-UiO-66 nano-MOFs: Revealing the effect of crystal size, sulfonation, and filler loading on the mechanical and conductivity properties. ACS Applied Materials & Interfaces, 2017, 9(48): 42239–42246
58. Liu M, Wang L, Zheng X, Xie Z. Zirconium-based nanoscale metal-organic framework/poly($\varepsilon$-caprolactone) mixed-matrix membranes as effective antimicrobials. ACS Applied Materials & Interfaces, 2017, 9(47): 41512–41520
59. Friebe S, Mundstock A, Volgmann K, Caro J. On the better understanding of the surprisingly high performance of metal-organic framework-based mixed-matrix membranes using the example of UiO-66 and Matrimid. ACS Applied Materials & Interfaces, 2017, 9(47): 41553–41558
60. Guan K, Zhao D, Zhang M, Shen J, Zhou G, Liu G, Jin W. 3D nanoporous crystals enabled 2D channels in graphene membrane with enhanced water purification performance. Journal of Membrane Science, 2017, 542: 41–51
61. Cheng X, Jiang X, Zhang Y, Lau C H, Xie Z, Ng D, Smith S J D, Hill M R, Shao L. Building additional passageways in polyamide membranes with hydrostable metal organic frameworks to recycle and remove organic solutes from various solvents. ACS Applied Materials & Interfaces, 2017, 9(44): 38877–38886
62. Yao B J, Ding L G, Li F, Li J T, Fu Q J, Ban Y, Guo A, Dong Y B. Chemically cross-linked MOF membrane generated from imidazolium-based ionic liquid-decorated UiO-66 type NMOF and its application toward $CO_2$ separation and conversion. ACS Applied Materials & Interfaces, 2017, 9(44): 38919–38930
63. Ma D, Han G, Peh S B, Chen S B. Water-stable metal-organic framework UiO-66 for performance enhancement of forward osmosis membranes. Industrial & Engineering Chemistry Research, 2017, 56(44): 12773–12782
64. Song Z, Qiu F, Zaia E W, Wang Z, Kunz M, Guo J, Brady M, Mi B, Urban J J. Dual-channel, molecular-sieving core/shell ZIF@-MOF architectures as engineered fillers in hybrid membranes for highly selective $CO_2$ separation. Nano Letters, 2017, 17(11): 6752–6758
65. Sun H, Tang B, Wu P. Development of hybrid ultrafiltration membranes with improved water separation properties using modified superhydrophilic metal-organic framework nanoparticles. ACS Applied Materials & Interfaces, 2017, 9(25): 21473–21484
66. Wang Z, Ren H, Zhang S, Zhang F, Jin J. Polymers of intrinsic microporosity/metal-organic framework hybrid membranes with improved interfacial interaction for high-performance $CO_2$ separation. Journal of Materials Chemistry. A, Materials for Energy and Sustainability, 2017, 5(22): 10968–10977
67. Xu Y M, Chung T S. High-performance UiO-66/polyimide mixed matrix membranes for ethanol, isopropanol and *n*-butanol dehydration via pervaporation. Journal of Membrane Science, 2017, 531: 16–26
68. Trinh D X, Tran T P N, Taniike T. Fabrication of new composite membrane filled with UiO-66 nanoparticles and its application to nanofiltration. Separation and Purification Technology, 2017, 177: 249–256
69. Ma J, Guo X, Ying Y, Liu D, Zhong C. Composite ultrafiltration membrane tailored by MOF@GO with highly improved water

purification performance. Chemical Engineering Journal, 2017, 313: 890–898

70. Guo X, Liu D, Han T, Huang H, Yang Q, Zhong C. Preparation of thin film nanocomposite membranes with surface modified MOF for high flux organic solvent nanofiltration. AIChE Journal. American Institute of Chemical Engineers, 2017, 63(4): 1303–1312
71. Castarlenas S, Téllez C, Coronas J. Gas separation with mixed matrix membranes obtained from MOF UiO-66-graphite oxide hybrids. Journal of Membrane Science, 2017, 526: 205–211
72. Ma D, Peh S B, Han G, Chen S B. Thin-film nanocomposite (TFN) membranes incorporated with super-hydrophilic metal-organic framework (MOF) UiO-66: Toward enhancement of water flux and salt rejection. ACS Applied Materials & Interfaces, 2017, 9(8): 7523–7534
73. Khdhayyer M R, Esposito E, Fuoco A, Monteleone M, Giorno L, Jansen J C, Attfield M P, Budd P M. Mixed matrix membranes based on UiO-66 MOFs in the polymer of intrinsic microporosity PIM-1. Separation and Purification Technology, 2017, 173: 304–313
74. Hu Z, Kang Z, Qian Y, Peng Y, Wang X, Chi C, Zhao D. Mixed matrix membranes containing UiO-66(Hf)-$(OH)_2$ metal-organic framework nanoparticles for efficient $H_2/CO_2$ separation. Industrial & Engineering Chemistry Research, 2016, 55(29): 7933–7940
75. Yao B J, Jiang W L, Dong Y, Liu Z X, Dong Y B. Post-synthetic polymerization of UiO-66-$NH_2$ nanoparticles and polyurethane oligomer toward stand-alone membranes for dye removal and separation. Chemistry (Weinheim an der Bergstrasse, Germany), 2016, 22(30): 10565–10571
76. Smith S J D, Lau C H, Mardel J I, Kitchin M, Konstas K, Ladewig B P, Hill M R. Physical aging in glassy mixed matrix membranes; tuning particle interaction for mechanically robust nanocomposite films. Journal of Materials Chemistry. A, Materials for Energy and Sustainability, 2016, 4(27): 10627–10634
77. Moreton J C, Denny M S, Cohen S M. High MOF loading in mixed-matrix membranes utilizing styrene/butadiene copolymers. Chemical Communications, 2016, 52(100): 14376–14379
78. Jiang W L, Ding L G, Yao B J, Wang J C, Chen G J, Li Y A, Ma J P, Ji J, Dong Y, Dong Y B. A MOF-membrane based on the covalent bonding driven assembly of a NMOF with an organic oligomer and its application in membrane reactors. Chemical Communications, 2016, 52(93): 13564–13567
79. Su N C, Sun D T, Beavers C M, Britt D K, Queen W L, Urban J J. Enhanced permeation arising from dual transport pathways in hybrid polymer–MOF membranes. Energy & Environmental Science, 2016, 9(3): 922–931
80. Armstrong M R, Arredondo K Y Y, Liu C Y, Stevens J E, Mayhob A, Shan B, Senthilnathan S, Balzer C J, Mu B. UiO-66 MOF and poly(vinyl cinnamate) nanofiber composite membranes synthesized by a facile three-stage process. Industrial & Engineering Chemistry Research, 2015, 54(49): 12386–12392
81. Anjum M W, Vermoortele F, Khan A L, Bueken B, De Vos D E, Vankelecom I F J. Modulated UiO-66-based mixed-matrix membranes for $CO_2$ separation. ACS Applied Materials & Interfaces, 2015, 7(45): 25193–25201
82. Smith S J D, Ladewig B P, Hill A J, Lau C H, Hill M R. Post-synthetic Ti exchanged UiO-66 metal-organic frameworks that deliver exceptional gas permeability in mixed matrix membranes. Scientific Reports, 2015, 5(1): 7823
83. Nik O G, Chen X Y, Kaliaguine S. Functionalized metal organic framework-polyimide mixed matrix membranes for $CO_2/CH_4$ separation. Journal of Membrane Science, 2012, 413–414: 48–61
84. Zhang Y, Feng X, Li H, Chen Y, Zhao J, Wang S, Wang L, Wang B. Photoinduced postsynthetic polymerization of a metal-organic framework toward a flexible stand-alone membrane. Angewandte Chemie International Edition, 2015, 54(14): 4259–4263
85. Kickelbick G, Feth M P, Bertagnolli H, Puchberger M, Holzinger D, Gross S. Formation of organically surface-modified metal oxo clusters from carboxylic acids and metal alkoxides: A mechanistic study. Journal of the Chemical Society, Dalton Transactions: Inorganic Chemistry, 2002, (20): 3892–3898
86. Liu X, Wang C, Wang B, Li K. Novel organic-dehydration membranes prepared from zirconium metal-organic frameworks. Advanced Functional Materials, 2017, 27(3): 1604311
87. Huang K, Wang B, Guo S, Li K. Micropatterned ultrathin MOF membranes with enhanced molecular sieving property. Angewandte Chemie International Edition, 2018, 57(42): 13892–13896
88. Zhang H, Hou J, Hu Y, Wang P, Ou R, Jiang L, Liu J Z, Freeman B D, Hill A J, Wang H. Ultrafast selective transport of alkali metal ions in metal organic frameworks with subnanometer pores. Science Advances, 2018, 4(2): eaaq0066
89. Wan L, Zhou C, Xu K, Feng B, Huang A. Synthesis of highly stable UiO-66-$NH_2$ membranes with high ions rejection for seawater desalination. Microporous and Mesoporous Materials, 2017, 252: 207–213
90. Wu F, Cao Y, Liu H, Zhang X. High-performance UiO-66-$NH_2$ tubular membranes by zirconia-induced synthesis for desulfurization of model gasoline via pervaporation. Journal of Membrane Science, 2018, 556: 54–65
91. Miyamoto M, Hori K, Goshima T, Takaya N, Oumi Y, Uemiya S. An organoselective zirconium-based metal-organic-framework UiO-66 membrane for pervaporation. European Journal of Inorganic Chemistry, 2017, 2017(14): 2094–2099
92. Liu J, Canfield N, Liu W. Preparation and characterization of a hydrophobic metal-organic framework membrane supported on a thin porous metal sheet. Industrial & Engineering Chemistry Research, 2016, 55(13): 3823–3832
93. Wu F, Lin L, Liu H, Wang H, Qiu J, Zhang X. Synthesis of stable UiO-66 membranes for pervaporation separation of methanol/methyl tert-butyl ether mixtures by secondary growth. Journal of Membrane Science, 2017, 544: 342–350
94. Wang X, Zhai L, Wang Y, Li R, Gu X, Yuan Y D, Qian Y, Hu Z, Zhao D. Improving water-treatment performance of zirconium metal-organic framework membranes by postsynthetic defect healing. ACS Applied Materials & Interfaces, 2017, 9(43): 37848–37855
95. Friebe S, Geppert B, Steinbach F, Caro J. Metal-organic framework UiO-66 layer: A highly oriented membrane with good selectivity and hydrogen permeance. ACS Applied Materials & Interfaces, 2017, 9(14): 12878–12885
96. Shan B, James J B, Armstrong M R, Close E C, Letham P A, Nikkhah K, Lin Y S, Mu B. Influences of deprotonation and

modulation on nucleation and growth of UiO-66: Intergrowth and orientation. Journal of Physical Chemistry C, 2018, 122(4): 2200–2206

97. Tsuruoka T, Furukawa S, Takashima Y, Yoshida K, Isoda S, Kitagawa S. Nanoporous nanorods fabricated by coordination modulation and oriented attachment growth. Angewandte Chemie International Edition, 2009, 48(26): 4739–4743
98. Schaate A, Roy P, Godt A, Lippke J, Waltz F, Wiebcke M, Behrens P. Modulated synthesis of Zr-based metal-organic frameworks: From nano to single crystals. Chemistry (Weinheim an der Bergstrasse, Germany), 2011, 17(24): 6643–6651
99. Zhang C, Zhao Y, Li Y, Zhang X, Chi L, Lu G. Defect-controlled preparation of UiO-66 metal-organic framework thin films with molecular sieving capability. Chemistry, an Asian Journal, 2016, 11(2): 207–210
100. Zhang Y, Zhao J, Wang K, Gao L, Meng M, Yan Y. Green synthesis of acid-base bi-functional UiO-66-type metal-organic frameworks membranes supported on polyurethane foam for glucose conversion. ChemistrySelect, 2018, 3(32): 9378–9387
101. Liang H, Jiao X, Li C, Chen D. Flexible self-supported metal–organic framework mats with exceptionally high porosity for enhanced separation and catalysis. Journal of Materials Chemistry. A, Materials for Energy and Sustainability, 2018, 6(2): 334–341
102. Lu A X, Ploskonka A M, Tovar T M, Peterson G W, DeCoste J B. Direct surface growth of UiO-66-$NH_2$ on polyacrylonitrile nanofibers for efficient toxic chemical removal. Industrial & Engineering Chemistry Research, 2017, 56(49): 14502–14506
103. Betke U, Proemmel S, Rannabauer S, Lieb A, Scheffler M, Scheffler F. Silane functionalized open-celled ceramic foams as support structure in metal organic framework composite materials. Microporous and Mesoporous Materials, 2017, 239: 209–220
104. Zhang X, Zhao Y, Mu S, Jiang C, Song M, Fang Q, Xue M, Qiu S, Chen B. UiO-66-coated mesh membrane with underwater super-oleophobicity for high-efficiency oil-water separation. ACS Applied Materials & Interfaces, 2018, 10(20): 17301–17308
105. Miyamoto M, Kohmura S, Iwatsuka H, Oumi Y, Uemiya S. *In situ* solvothermal growth of highly oriented Zr-based metal organic framework UiO-66 film with monocrystalline layer. CrystEngComm, 2015, 17(18): 3422–3425
106. Lausund K B, Nilsen O. All-gas-phase synthesis of UiO-66 through modulated atomic layer deposition. Nature Communications, 2016, 7(1): 13578
107. Lausund K B, Petrovic V, Nilsen O. All-gas-phase synthesis of amino-functionalized UiO-66 thin films. Dalton Transactions (Cambridge, England), 2017, 46(48): 16983–16992
108. Virmani E, Rotter J M, Mähringer A, von Zons T, Godt A, Bein T, Wuttke S, Medina D D. On-surface synthesis of highly oriented thin metal-organic framework films through vapor-assisted conversion. Journal of the American Chemical Society, 2018, 140(14): 4812–4819
109. Hod I, Bury W, Karlin D M, Deria P, Kung C W, Katz M J, So M, Klahr B, Jin D, Chung Y W, et al. Directed growth of electroactive metal-organic framework thin films using electrophoretic deposition. Advanced Materials, 2014, 26(36): 6295–6300
110. Stassen I, Styles M, Van Assche T, Campagnol N, Fransaer J, Denayer J, Tan J C, Falcaro P, De Vos D, Ameloot R. Electrochemical film deposition of the zirconium metal-organic framework UiO-66 and application in a miniaturized sorbent trap. Chemistry of Materials, 2015, 27(5): 1801–1807
111. Shangkum G, Chammingkwan P, Trinh D, Taniike T. Design of a semi-continuous selective layer based on deposition of UiO-66 nanoparticles for nanofiltration. Membranes, 2018, 8(4): 129
112. Ghorbanpour A, Huelsenbeck L D, Smilgies D M, Giri G. Oriented UiO-66 thin films through solution shearing. CrystEngComm, 2018, 20(3): 294–300
113. Kosinov N, Gascon J, Kapteijn F, Hensen E J M. Recent developments in zeolite membranes for gas separation. Journal of Membrane Science, 2016, 499: 65–79
114. Piszczek P, Radtke A, Grodzicki A, Wojtczak A, Chojnacki J. The new type of $[Zr_6(\mu3\text{-}O)_4(\mu3\text{-}OH)_4]$ cluster core: Crystal structure and spectral characterization of $[Zr_6O_4(OH)_4(OOCR)_{12}]$ (R = But, $C(CH_3)_2Et$). Polyhedron, 2007, 26(3): 679–685
115. Yao H B, Yan Y X, Gao H L, Vaughn J, Pappas I, Masters J G, Yuan S, Yu S H, Pan L. An investigation of zirconium(iv)–glycine (CP-2) hybrid complex in bovine serum albumin protein matrix under varying conditions. Journal of Materials Chemistry, 2011, 21 (47): 19005–19012
116. van der Drift A. Evolutionary selection, a principle governing growth orientation in vapour-deposited layers. Philips Research Reports, 1967, 22: 267–288
117. Lu G, Cui C, Zhang W, Liu Y, Huo F. Synthesis and self-assembly of monodispersed metal-organic framework microcrystals. Chemistry, an Asian Journal, 2013, 8(1): 69–72
118. Miikkulainen V, Leskelä M, Ritala M, Puurunen R L. Crystallinity of inorganic films grown by atomic layer deposition: Overview and general trends. Journal of Applied Physics, 2013, 113(2): 021301
119. Ma X, Kumar P, Mittal N, Khlyustova A, Daoutidis P, Mkhoyan K A, Tsapatsis M. Zeolitic imidazolate framework membranes made by ligand-induced permselectivation. Science, 2018, 361(6406): 1008–1011
120. Stassen I, Styles M, Grenci G, Gorp Hans V, Vanderlinden W, Feyter Steven D, Falcaro P, Vos D D, Vereecken P, Ameloot R. Chemical vapour deposition of zeolitic imidazolate framework thin films. Nature Materials, 2015, 15(3): 304–310
121. Li W, Su P, Li Z, Xu Z, Wang F, Ou H, Zhang J, Zhang G, Zeng E. Ultrathin metal-organic framework membrane production by gel-vapour deposition. Nature Communications, 2017, 8(1): 406
122. Lin H, Zhu Q, Shu D, Lin D, Xu J, Huang X, Shi W, Xi X, Wang J, Gao L. Growth of environmentally stable transition metal selenide films. Nature Materials, 2019, 18(6): 602–607
123. Falcaro P, Ricco R, Doherty C M, Liang K, Hill A J, Styles M J. MOF positioning technology and device fabrication. Chemical Society Reviews, 2014, 43(16): 5513–5560
124. Ameloot R, Stappers L, Fransaer J, Alaerts L, Sels B F, De Vos D E. Patterned growth of metal-organic framework coatings by electrochemical synthesis. Chemistry of Materials, 2009, 21(13): 2580–2582
125. Li M, Dincă M. Reductive electrosynthesis of crystalline metal-organic frameworks. Journal of the American Chemical Society, 2011, 133(33): 12926–12929
126. Wu W, Li Z, Chen Y, Li W. Polydopamine-modified metal-organic framework membrane with enhanced selectivity for carbon

capture. Environmental Science & Technology, 2019, 53(7): 3764–3772

127. Devautour-Vinot S, Martineau C, Diaby S, Ben-Yahia M, Miller S, Serre C, Horcajada P, Cunha D, Taulelle F, Maurin G. Caffeine confinement into a series of functionalized porous zirconium MOFs: A joint experimental/modeling exploration. Journal of Physical Chemistry C, 2013, 117(22): 11694–11704
128. Valenzano L, Civalleri B, Chavan S, Bordiga S, Nilsen M H, Jakobsen S, Lillerud K P, Lamberti C. Disclosing the complex structure of UiO-66 metal organic framework: A synergic combination of experiment and theory. Chemistry of Materials, 2011, 23(7): 1700–1718
129. Wu H, Chua Y S, Krungleviciute V, Tyagi M, Chen P, Yildirim T, Zhou W. Unusual and highly tunable missing-linker defects in zirconium metal-organic framework UiO-66 and their important effects on gas adsorption. Journal of the American Chemical Society, 2013, 135(28): 10525–10532
130. Trickett C A, Gagnon K J, Lee S, Gándara F, Bürgi H B, Yaghi O M. Definitive molecular level characterization of defects in UiO-66 crystals. Angewandte Chemie International Edition, 2015, 54(38): 11162–11167
131. Brown A J, Brunelli N A, Eum K, Rashidi F, Johnson J R, Koros W J, Jones C W, Nair S. Interfacial microfluidic processing of metal-organic framework hollow fiber membranes. Science, 2014, 345(6192): 72–75
132. DeStefano M R, Islamoglu T, Garibay S J, Hupp J T, Farha O K. Room-temperature synthesis of UiO-66 and thermal modulation of densities of defect sites. Chemistry of Materials, 2017, 29(3): 1357–1361
133. Hu Z, Peng Y, Kang Z, Qian Y, Zhao D. A modulated hydrothermal (MHT) approach for the facile synthesis of UiO-66-type MOFs. Inorganic Chemistry, 2015, 54(10): 4862–4868